Phase Equilibria in the Fe-Mo-Ti Ternary System at 1173 K (900 °C) and 1023 K (750 °C)

A.J. KNOWLES, N.G. JONES, C.N. JONES, and H.J. STONE

Alloys with fine-scale eutectic microstructures comprising Ti-based A2 and TiFe B2 phases have been shown to have excellent mechanical properties. In this study, the potential of alloys with further refined A2-B2 microstructures formed through solid-state precipitation has been explored by analyzing a series of six alloys within the Fe-Mo-Ti ternary system. Partial isothermal sections of this system at 1173 K (900 °C) and 1023 K (750 °C) were constructed, from which the ternary solubility limits of the A2 (Ti, Mo), B2 TiFe, $D8_5$ Fe_7Mo_6, and C14 Fe_2Ti phases were determined. With these data, the change in solubility of Fe in the A2 phase with temperature, which provides the driving force for precipitation of B2 TiFe, was determined and used to predict the maximum potential volume fraction of B2 TiFe precipitates that may be formed in an A2 (Ti, Mo) matrix.

DOI: 10.1007/s11661-017-4134-6

I. INTRODUCTION

TERNARY Ti-Fe-X eutectic alloys (X = Nb, V, Sn) comprising two-phase microstructures of A2 (Ti, X) and B2 TiFe phases are believed to have potential for structural applications. These alloys have been shown to possess strengths up to 2 GPa and elongations to failure of 15 pct.[1–5] An alternative approach by which a microstructure containing these phases can be generated is through precipitation of the B2 phase from an A2 matrix. This approach is attractive as it offers the possibility of greater microstructural control than can be achieved through an invariant reaction. A recent study of Fe-Mo-Ti alloys has shown that such precipitation can generate two-phase microstructures with finer dispersions of the A2 and B2 phases than have been reported in the eutectic alloys.[6] However, determining the limits to which such precipitation may be exploited requires an improved understanding of the phase equilibria in the Ti-rich corner of this ternary system.

Isothermal sections of the Fe-Mo-Ti ternary system at 1273 K (1000 °C) have been constructed from experimental studies of diffusion multiples[7] and bulk alloys.[8] These studies have established how the solubility of Fe in A2 (Ti, Mo) varies with the Ti:Mo ratio and the amount of Mo that may be accommodated in the B2 TiFe phase at this temperature. In addition, predicted isothermal sections indicate that the extent to which the solubility of Fe in A2 (Ti, Mo) changes with temperature between 1123 K (850 °C) and 1373 K (1100 °C) is strongly dependent upon the Ti:Mo ratio.[7] However, very little experimental data exist regarding the phase equilibria at temperatures other than 1273 K (1000 °C), and those studies that have been performed have considered only limited ranges of ternary composition space.[9–14]

To address this issue, the phase equilibria that exist in the Mo-Ti-rich region of the Fe-Mo-Ti ternary system have been determined by examining a series of bulk alloy samples following extended heat treatments at 1173 K (900 °C) and 1023 K (750 °C). These data have been used to construct vertical sections between the A2 (Ti, Mo) and B2 TiFe phases, for Mo additions of up to 40 at. pct, which are essential for determining the extent to which precipitation may occur in alloys based on this system.

II. EXPERIMENTAL METHODS

Six alloys, with target compositions given in Table I, were prepared by arc melting of elemental metals with purity ≥99.9 pct. Melting was performed in an evacuated and Ar-backfilled atmosphere and each ingot was inverted and remelted five times in order to improve compositional homogeneity. Ingots were approximately 60 mm in length and 10 mm in diameter, with a total mass of 40 g. Sections from each ingot, ~10 mm in length, were encapsulated in evacuated, argon-backfilled quartz ampoules, which also contained Ti granules to remove any residual oxygen remaining in the atmosphere. The encapsulated samples were heat treated for

A.J. KNOWLES, N.G. JONES, and H.J. STONE are with the Department of Materials Science and Metallurgy, University of Cambridge, Cambridge, CB3 0FS, U.K. Contact e-mail: hjs1002@cam.ac.uk C.N. JONES is with Rolls-Royce plc, P.O.Box 31, Derby, DE24 8BJ, U.K.

Manuscript submitted July 29, 2016.
Article published online July 5, 2017

either 500 hours at 1173 K (900 °C) or 1000 hours at 1023 K (750 °C). All samples were water quenched at the end of the heat treatment process.

X-ray diffraction (XRD) of the heat-treated samples was conducted using a Bruker D8 diffractometer with a Cu target operated at 40 kV and 40 mA. Each pattern was collected between angles of 20 deg and 80 deg 2θ, with a step size of 0.03 deg 2θ, over a 2 hour period. Solid slices of the arc-melted ingot were used, ~10 mm in diameter and ~1 mm thickness. Owing to the arc melting and long-duration heat treatment, the average grain size was large, ~150 μm, resulting in non-powder average XRD patterns.

Microstructural characterization was performed using scanning electron microscopy (SEM) in either a JEOL 5800 or an FEI Nova NanoSEM, both operated at an accelerating voltage of 20 kV. Compositional analyses were performed by energy-dispersive X-ray spectroscopy (EDX) in the same instruments. Bulk alloy compositions were determined by averaging three 200×400 μm area scans collected from different regions of the ingots. Similarly, phase compositions were obtained from the average of five individual point analyses. Where possible, point analyses were performed close to the interface between adjacent phases, making use of the local equilibria that exist in these regions. For both bulk and phase compositions, the standard deviation in the measurements has been presented as the error.

III. RESULTS AND DISCUSSION

The experimentally determined bulk compositions of the alloys are given in Table I. Despite some significant differences between the measured and target compositions, the alloys still provided effective coverage of the region of interest in ternary space.

A. *X-ray Diffraction*

X-ray diffraction patterns collected from the alloys following heat treatment at 1173 K (900 °C) and 1023 K (750 °C) are shown in Figures 1 and 2, respectively. The phases identified in each of the alloys were found to be consistent between the two temperatures. Strong reflections corresponding to an A2 phase were identified in all of the patterns, except that of alloy TF60M10, where the A2 reflections were weak. The A2 reflections obtained from alloys TF20M10, TF20M20, and TF20M40 exhibited some shouldering at lower diffraction angles, suggesting the presence of an additional phase. Previous investigations of these alloys following heat treatment at 1273 K (1000 °C) identified similar features in the X-ray diffraction patterns.[8] In that study, selected area diffraction patterns obtained using transmission electron microscopy were observed to contain reflections consistent with the metastable incommensurate omega phase, which is known to form in the A2 phase on rapid cooling in Ti-Fe-based alloys.[15,16] Based on this work, the shoulders to lower angles observed on the A2 reflections in the present work are similarly believed to correspond to the presence of an omega phase with somewhat larger plane spacing than the parent A2 phase, with the peaks broadened as a result of the fine crystallite size.[8]

In addition to reflections from the A2 phase, the X-ray diffraction patterns collected from alloys TF20M10, TF20M20, and TF20M40 were also found to contain strong reflections from a B2 phase. Additional reflections were also observed in the patterns acquired from alloys TF20M60 and TF20M70, which were consistent with the presence of a $D8_5$ phase. Similarly, reflections indicative of a C14 phase were observed in the patterns acquired from alloy TF60M10. The patterns obtained from alloys TF20M60 and TF20M70 also contained additional weak reflections, which were believed to be associated with the presence of small quantities of the C14 phase, as has been reported in these alloys following heat treatment at 1273 K (1000 °C).[8] Weak reflections were also observed in the patterns acquired from alloy TF60M10, believed to be indicative of a low volume fraction of the $D8_5$ phase. Quantitative analysis of the phases present using Rietveld refinement was not possible because of the large grain sizes generated through the arc melting and heat treatment processes, which meant that the diffraction patterns did not display powder-averaged intensities.

Pawley peak fitting of the A2 phase within both alloys TF20M10 and TF20M20 found them both to have similar lattice parameters of 3.16 ± 0.01 Å at 1173 K (900 °C) and 3.18 ± 0.01 Å at 1023 K (750 °C). The B2 phases were also found to have similar lattice

Table I. Alloy Designations, Target Compositions, and Compositions Measured by EDX Area Scans

	Target Composition (At. Pct)			Measured Composition (At. Pct)		
Alloy	Ti	Fe	Mo	Ti	Fe	Mo
TF20M10	70	20	10	70.6 ± 0.4	18.5 ± 0.3	10.9 ± 0.5
TF20M20	60	20	20	58.5 ± 0.4	16.4 ± 1.4	25.1 ± 1.0
TF20M40	40	20	40	37.1 ± 1.8	16.3 ± 1.7	46.7 ± 0.1
TF20M60	20	20	60	16.3 ± 1.7	19.4 ± 1.0	64.3 ± 2.7
TF20M70	10	20	70	9.7 ± 0.3	17.5 ± 1.2	72.8 ± 1.5
TF60M10	30	60	10	30.4 ± 0.8	57.6 ± 1.8	12.0 ± 2.6

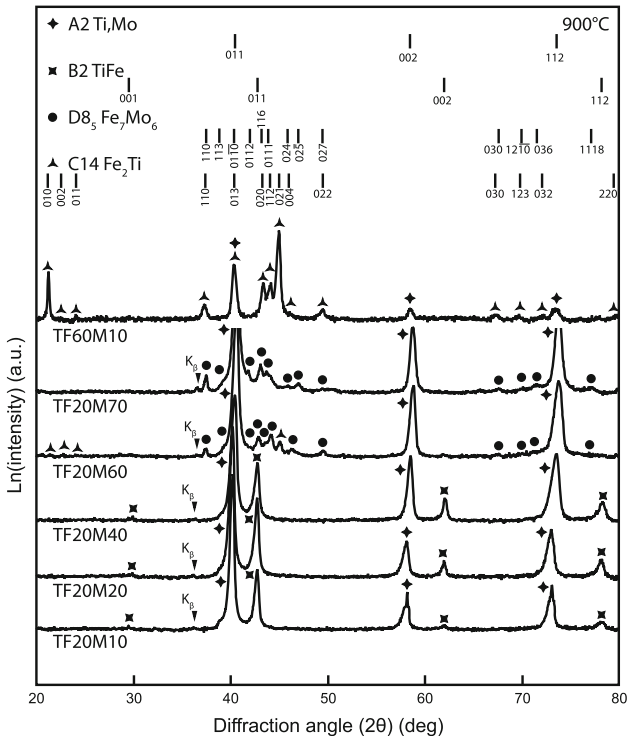

Fig. 1—X-ray diffraction patterns of the alloys following heat treatment at 1173 K (900 °C).

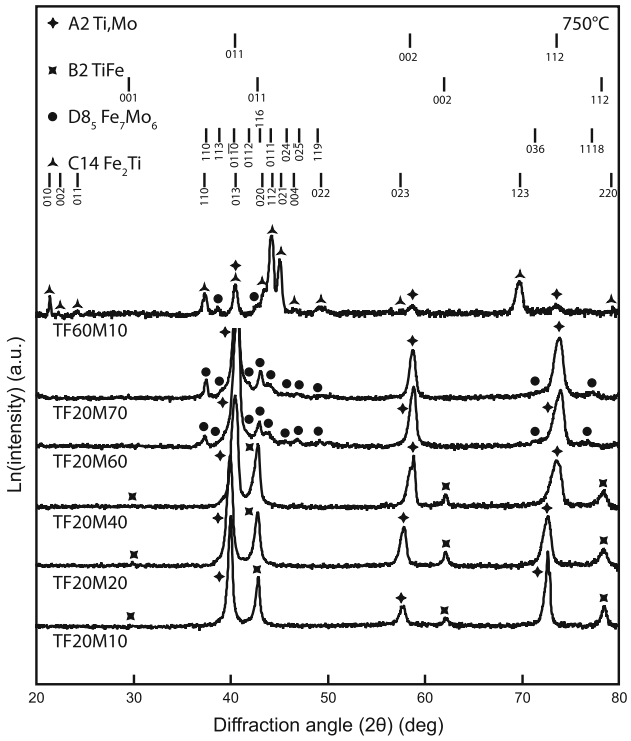

Fig. 2—X-ray diffraction patterns of the alloys following heat treatment at 1023 K (750 °C).

parameters in the two alloys of 2.98 ± 0.01 Å at 1173 K (900 °C) and 2.97 ± 0.01 Å at 1023 K (750 °C). In the TF20M40 alloy, the A2 phase was found to have a somewhat lower lattice parameter of 3.15 ± 0.01 Å at 1173 K (900 °C) and 3.14 ± 0.01 Å at 1023 K (750 °C). While those of the B2 phase in alloy TF20M40 of 2.98 ± 0.01 Å at 1173 K (900 °C) and 2.97 ± 0.01 Å at 1023 K (750 °C) were similar to those in the TF20M10 and TF20M20 alloys.

B. *Microstructural Characterization*

Backscattered electron (BSE) micrographs of the alloys following heat treatment at 1173 K (900 °C) and 1023 K (750 °C) are shown in Figures 3 and 4, respectively. The microstructures of each alloy following exposure at the two temperatures were broadly similar. The five alloys nominally containing 20 at. pct Fe had compositions that lay close to the A2 single-phase field boundary, when plotted on the 1273 K (1000 °C) isothermal sections reported in References 7 and 8. As a result, these alloys would be expected to contain primary A2 dendrites, rich in Ti and Mo, evidence of which can be seen in Figures 3 and 4.

In alloys TF20M10 and TF20M20, a darker contrast interdendritic phase was observed between the brighter contrast primary dendrites. A variation in contrast could also be observed across the dendrites of alloy TF20M20 following heat treatment at 1023 K (750 °C), which suggested minor coring remained in the microstructure as a result of solidification-induced microsegregation. The results of the EDX phase analysis, performed close to their interfaces to make use of local equilibria, are summarized in Tables II and III. These data confirmed that the brighter contrast dendrites were rich in Ti and Mo, while the darker contrast interdendritic phase had near equiatomic concentrations of Ti and Fe. These compositions were similar to those reported previously for the A2 and B2 phases in these alloys,[8] and are consistent with the X-ray diffraction data shown in Figures 1 and 2. The decreased Fe solubility (see Tables II and III) is consistent with the slight increase in the A2 lattice parameter from 1173 K (900 °C) to 1023 K (750 °C).

The microstructure of alloy TF20M40 contained a coarse dendritic structure of brighter contrast primary dendrites and a darker contrast interdendritic phase. However, unlike alloys TF20M10 and TF20M20, fine-scale precipitates were observed within these phases. Following heat treatment at 1173 K (900 °C), Figure 3(c) and (d), bright contrast precipitates were present within the interdendritic phase, while darker contrast features were found in the brighter contrast dendrites. In comparison, after heat treatment at 1023 K (750 °C), Figure 4(c) and (d), precipitates were only observed in the interdendritic phase. These precipitates were more refined than those seen following exposure at 1173 K (900 °C), as would be expected following heat treatment at a lower temperature. Compositional analysis of the fine-scale precipitates was not possible in the SEM because of the relatively large probe size of ~1 μm. X-ray diffraction data from this alloy indicated that it contained only A2 and B2 phases. As such, it is believed that the darker contrast precipitates within the dendrites are the B2 phase, while the brighter contrast precipitates within the interdendritic constituent are the A2 phase. This was consistent with the

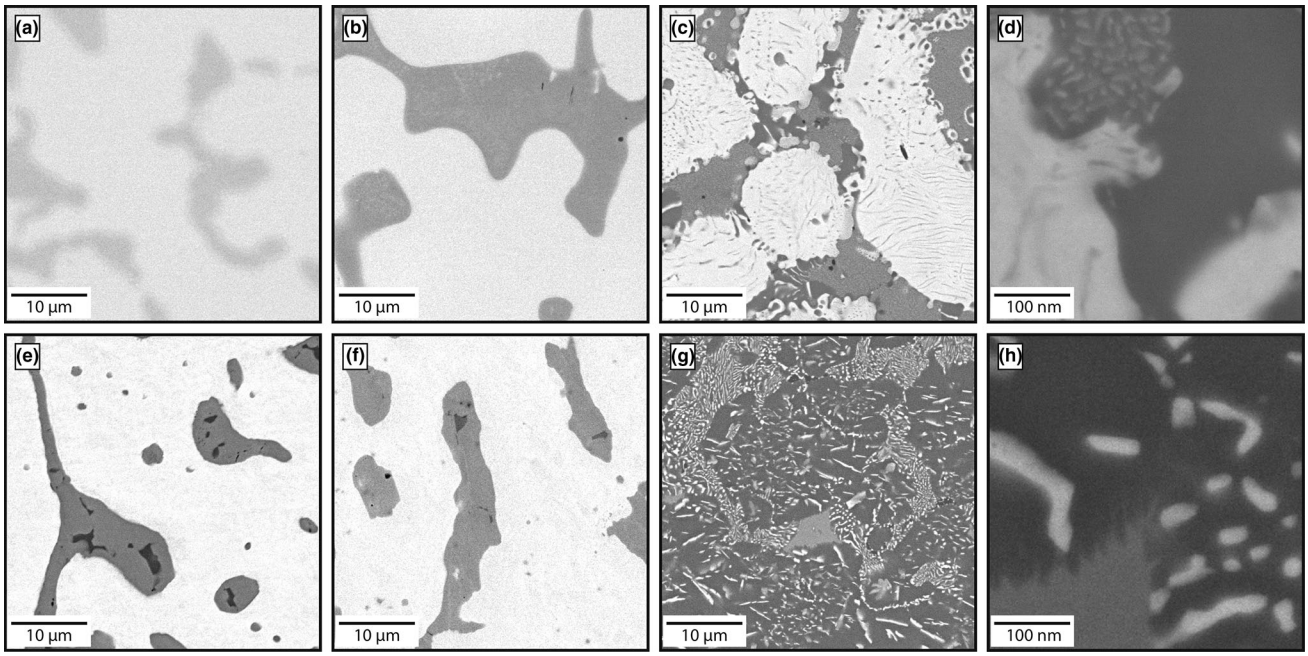

Fig. 3—BSE micrographs of the alloys following heat treatment at 1173 K (900 °C): (*a*) TF20M10, (*b*) TF20M20, (*c*) TF20M40 overview and (*d*) detailed view, (*e*) TF20M60, (*f*) TF20M70, (*g*) TF60M10 overview, and (*h*) detailed view.

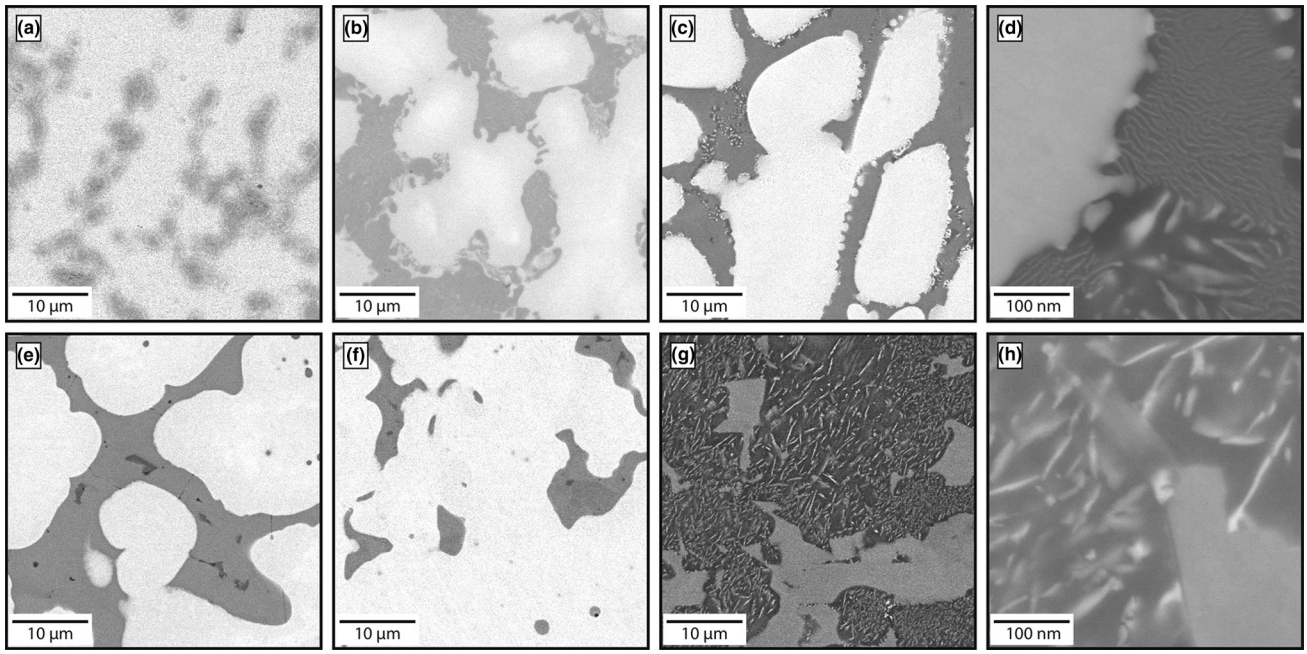

Fig. 4—BSE micrographs of the alloys following heat treatment at 1023 K (750 °C): (*a*) TF20M10, (*b*) TF20M20, (*c*) TF20M40 overview and (*d*) detailed view, (*e*) TF20M60, (*f*) TF20M70, (*g*) TF60M10 overview, and (*h*) detailed view.

precipitates having a similar BSE contrast to the corresponding coarse interdendritic B2 phase and is further supported by transmission electron microscopy data presented in Reference 8. The lattice parameters of the A2 phases within alloy TF20M40 at 1173 K (900 °C) and 1023 K (750 °C) were somewhat lower than for the A2 phase in the TF20M10 and TF20M20 alloys, principally as a consequence of the reduced Fe solubility (see Tables II and III). While the similarity of the lattice parameters of the B2 phases within the TF20M10, TF20M20, and TF20M40 alloys suggested that the B2 phases had a similar composition within each of the three alloys.

The microstructures of alloys TF20M60, Figures 3(e) and 4(e), and TF20M70, Figures 3(f) and 4(f), contained three distinct phases. In both alloys, brighter contrast primary dendrites dominated the microstructure, interspersed by a darker contrast interdentritic constituent.

Table II. Phases Present in the Alloys Heat Treated at 1173 K (900 °C) Determined by XRD and Their Compositions Determined by EDX

Alloy	Phase	Ti (At. Pct)	Fe (At. Pct)	Mo (At. Pct)
TF20M10	A2	72.3 ± 0.3	14.8 ± 0.2	12.9 ± 0.5
	B2	51.4 ± 0.2	47.3 ± 0.3	1.3 ± 0.2
TF20M20	A2	60.7 ± 0.4	9.2 ± 0.4	30.1 ± 0.8
	B2	51.3 ± 0.4	45.2 ± 1.3	3.5 ± 1.0
TF20M40	A2	34.6 ± 2.6	5.2 ± 1.4	60.3 ± 3.1
	B2	49.5 ± 1.9	45.0 ± 3.0	5.5 ± 2.0
TF20M60	A2	17.4 ± 1.0	3.7 ± 2.2	78.9 ± 1.4
	$D8_5$	26.6 ± 0.4	52.1 ± 0.8	21.3 ± 1.2
TF20M70	A2	7.6 ± 0.2	6.8 ± 0.5	85.6 ± 0.6
	$D8_5$	15.8 ± 0.6	54.4 ± 0.6	29.8 ± 1.2
TF60M10	C14	31.5 ± 0.3	63.6 ± 0.8	4.9 ± 0.8
	$D8_5$	29.0 ± 0.7	49.8 ± 1.5	21.2 ± 1.1

Table III. Phases Present in the Alloys Heat Treated at 1023 K (750 °C) Determined by XRD and Their Compositions Determined by EDX

Alloy	Phase	Ti (At. Pct)	Fe (At. Pct)	Mo (At. Pct)
TF20M10	A2	75.3 ± 0.6	11.7 ± 0.4	13.0 ± 0.5
	B2	53.8 ± 2.1	44.5 ± 3.2	1.7 ± 1.2
TF20M20	A2	62.8 ± 0.6	6.4 ± 0.4	30.8 ± 1.0
	B2	52.4 ± 0.6	44.6 ± 1.3	2.9 ± 1.0
TF20M40	A2	33.0 ± 1.3	6.8 ± 0.2	60.2 ± 1.2
	B2	47.7 ± 0.3	40.6 ± 1.3	11.7 ± 1.1
TF20M60	A2	13.3 ± 0.6	8.6 ± 1.2	78.1 ± 1.2
	$D8_5$	25.2 ± 1.5	52.8 ± 0.8	22.0 ± 1.1
TF20M70	A2	7.7 ± 0.4	7.4 ± 1.5	84.9 ± 1.9
	$D8_5$	15.3 ± 0.4	53.5 ± 0.5	31.1 ± 0.6
TF60M10	C14	31.1 ± 0.4	58.4 ± 0.3	10.5 ± 0.6
	$D8_5$	27.9 ± 0.2	51.2 ± 0.3	20.9 ± 0.2

However, unlike the alloys discussed previously, isolated occurrences of an even darker contrast phase were observed within the interdendritic regions. Compositional analysis using EDX indicated that the brighter dendrites were predominately Mo. While in contrast to the alloys discussed previously, the principal interdendritic constituent was rich in Fe but did not contain similar levels of Ti. Reliable EDX data could not be obtained from the darkest phase within the interdendritic regions because of its relatively small size. However, measurements including these features indicated that they were lean in Mo when compared to the surrounding material. Overlaying the measured phase compositions on the 1273 K (1000 °C) isothermal sections[7,8] suggested that the primary dendrites were the A2 phase, while the principal interdendritic constituent was the $D8_5$ phase. This is consistent with the X-ray diffraction data presented in Figures 1 and 2. As discussed above, the X-ray data from these alloys also contained weak reflections from a C14 phase, and it is believed that this corresponded to the isolated regions of darkest BSE contrast, located within the principal interdendritic constituent. The lower Mo content of these features compared to the surrounding material also supports this interpretation. Despite the nominal compositions of these alloys lying within the A2-$D8_5$ two-phase region, previous studies have suggested that solidification-based microsegregation may allow local enrichment of Fe in the interdendritic material, resulting in a different local phase equilibrium between the $D8_5$ and C14 phases.[8] While the true phase equilibria of these alloys lies in the A2-$D8_5$ two-phase field, the low diffusion kinetics associated with complex intermetallic phases, such as the $D8_5$ phase, are likely to require considerably extended heat treatments to fully repartition the elements and eliminate the C14 phase.

Following heat treatment at both 1173 K (900 °C) and 1023 K (750 °C), alloy TF60M10 displayed a markedly different microstructure to all the other alloys examined, Figure 3(g) and (h) as well as Figure 4(g) and (h). The primary dendrites had a darker contrast than the gray interdendritic constituent and contained brighter contrast acicular precipitates. The microstructures at both temperatures were similar, although a greater volume fraction of the interdendritic constituent was observed following heat treatment at 1023 K (750 °C), along with finer bright contrast precipitates. The composition of the dendritic and interdendritic phases, determined by EDX, were consistent with the C14 and $D8_5$ phases reported previously.[7,8] This was further supported by the X-ray diffraction data presented in Figures 1 and 2, which identified reflections from C14 and $D8_5$ phases. The X-ray data also indicated the presence of an A2 phase in this alloy, which is believed to be the acicular precipitates. The bright BSE contrast of these precipitates is consistent with a high

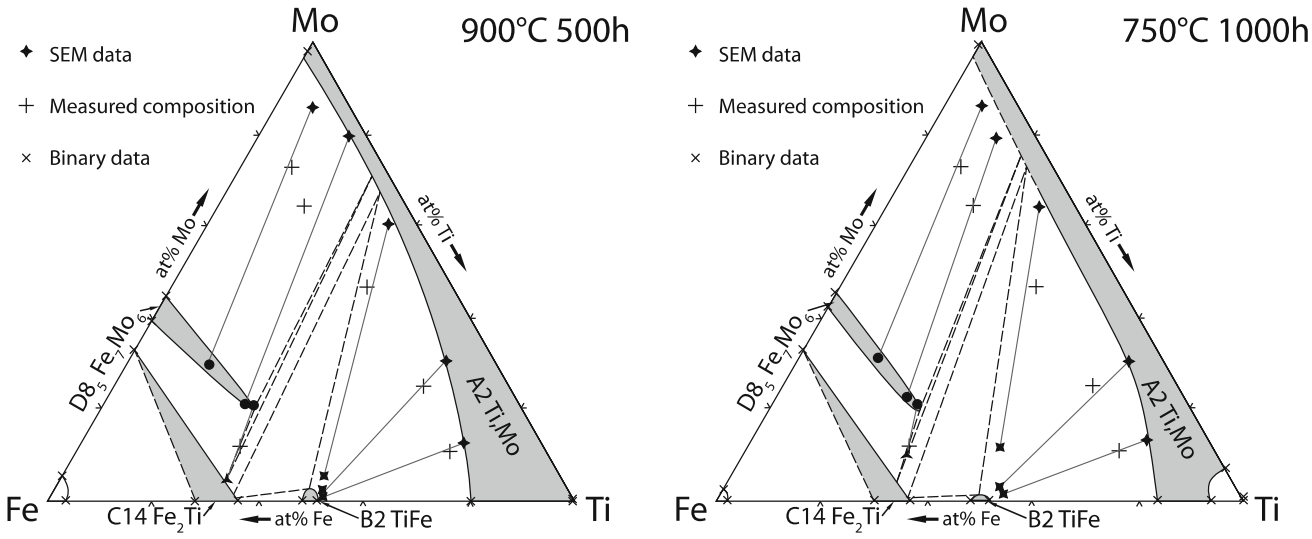

Fig. 5—Fe-Mo-Ti ternary isothermal sections at 1173 K (900 °C) and 1023 K (750 °C).

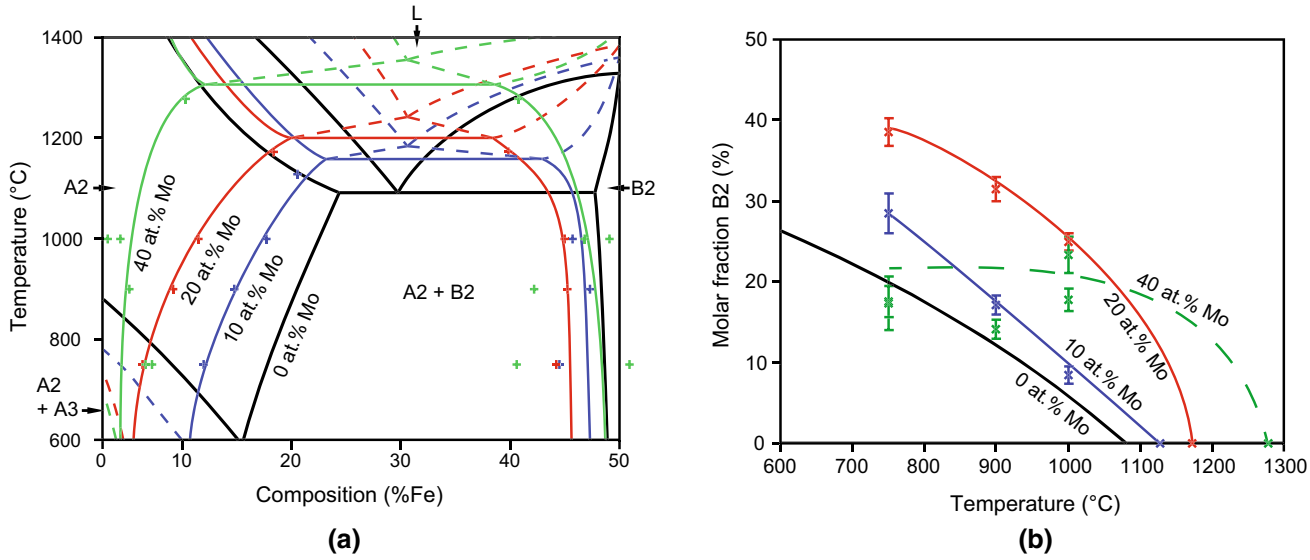

Fig. 6—(*a*) Vertical sections from A2 (Ti, Mo) to B2 TiFe, and (*b*) predicted B2 molar fraction with temperature.

Mo concentration, as may be expected in such an A2 phase. Critically, it should be noted that the A2 phase was predominately found within the C14 dendrites, with only limited occurrences of three-phase triple points. This suggests that the bulk composition of the alloy was within the C14-D8$_5$ two-phase field and that the formation of the A2 phase occurred as a result of solute partitioning during the solidification of C14 dendrites, leading to a composition of the C14 phase that was within the C14-A2 two-phase field at lower temperatures.

C. *Isothermal Sections at 1173 K (900 °C) and 1023 K (750 °C)*

Partial isothermal sections from the Ti- and Mo-rich region of Fe-Mo-Ti ternary system at 1173 K (900 °C) and 1023 K (750 °C) were constructed using the compositions of the phases measured in this study, Figure 5. Data from previous assessments of the bounding Fe-Ti,[17] Mo-Ti,[18] and Fe-Mo[19] binary systems were also incorporated. Where possible, tie lines were drawn between phases that were found to be in equilibrium. In addition, the continuous C14 phase field reported by Sokolovskaya *et al.*[11] from Fe_2Ti to Fe_2Mo at 1173 K (900 °C) was included, as well as the Ti-rich A2-A3 two-phase field at 1023 K (750 °C) proposed by Shurin *et al.*[13]

At both 1173 K (900 °C) and 1023 K (750 °C), the A2 phase field was found to be continuous between Ti and Mo, with the solubility of Fe in this phase decreasing with increasing Mo content. For Ti-rich A2 compositions, good agreement was observed between the limit of solubility of Fe and that reported in the Fe-Ti binary system.[20,21] In contrast, higher Fe concentrations were found in the Mo-rich A2 phase than reported in the

Fe-Mo binary system.[22,23] This was particularly pronounced in alloys TF20M60 and TF20M70 following heat treatment at 1023 K (750 °C) where the 1000 hour heat treatment period may not have been sufficient to reach equilibrium conditions. The heat treatment periods were comparable to the 480 hours at 1273 K (1000 °C) used in the Ti-Fe-Mo ternary work of Jin and Qiu,[7] as well as the 67 days at 1173 K (900 °C) made in the binary Fe-Mo determination by Heijwegen and Rieck.[23]

The TiFe B2 showed limited solubility for Mo, which was lower than that reported by Sokolovkaya *et al.*[11] but higher than that suggested in the work of Jin and Qiu.[7] However, caution must be exercised, as EDX measurements of the B2 phase may have also sampled the fine A2 phase. This is particularly true for alloy TF20M40 following heat treatment at 1023 K (750 °C), where the precipitates were very fine and the B2 phase difficult to sample in isolation. At both 1173 K (900 °C) and 1023 K (750 °C), the $D8_5$ phase field was found to have significant solubility for Ti, following the formula $Fe_7(Ti, Mo)_6$, which is consistent with that proposed in Reference 7. However, the limit of solubility for Ti in this phase, ~25 at. pct in the present work, is significantly larger than the previous report of ~14 at. pct Ti at 1273 K (1000 °C).[7]

D. *Vertical Sections and B2 TiFe Molar Fraction Prediction*

Combining data from the present work, with previously published ternary[6–8] and Fe-Ti binary[24] studies, enabled vertical sections between the A2 (Ti, Mo) and B2 TiFe phases to be plotted, Figure 6(a). The maximum solubility for Fe in the A2 phase was seen to reduce as the Mo content increased. The solubility for Fe in the A2 phase was also observed to decrease markedly at lower temperatures.

While the data appear to suggest that the concentration of Fe in the B2 phase decreases with increasing Mo content, for alloys up to 20 at. pct Mo, and that higher concentrations of Fe are accommodated with 40 at. pct Mo, the scatter in the data prohibits definitive conclusions being drawn. The origin of this uncertainty is the difficulty in determining the composition of the B2 phase in isolation, without simultaneously sampling fine A2 precipitates.

The solidus temperature of Ti-20Fe-xMo (x = 10, 20, 40) at. pct alloys have previously been reported to increase with Mo content.[6] Assuming that the eutectic form of the binary Fe-Ti phase diagram does not change with Mo substitutions for Ti, then these solidus temperatures are likely to be representative of the eutectic temperatures. The A2 → A3 transitions, liquidus temperatures, and A2 + B2 + L three-phase fields were not determined within this study and so are shown as dashed lines.

The reduced solubility of Fe in the A2 (Ti, Mo) phase with decreasing temperature can be used to generate microstructures comprising an A2 (Ti, Mo) matrix with B2 TiFe precipitates.[6] Using the A2 and B2 phase boundaries plotted in Figure 6(a), the maximum molar fraction of B2 precipitates that may be formed in an A2 matrix at a given temperature was calculated, Figure 6(b). As would be expected, the maximum molar fraction of precipitates increases as temperature decreases for all the alloys considered. In addition, for a given temperature, the maximum molar fraction of B2 precipitates increases with Mo concentration up to 20 at. pct. With higher Mo contents, a lower maximum B2 molar fraction is attained, as shown by the data for 40 at. pct Mo. This behavior may be attributed to the lower solubility of Fe in the A2 phase at the solidus temperature of this alloy and the smaller change in Fe solubility with respect to temperature. While the data indicate that this transition occurs between 20 and 40 at. pct Mo, the precise composition that would lead to the maximum possible molar fraction of the B2 phase could not be determined from the data acquired. It should be noted that simply increasing the volume fraction of the B2 precipitates would not necessarily lead to a corresponding improvement of the mechanical properties. For example, previous work has shown that greater Mo concentrations alter the morphology and size of the B2 precipitates, resulting in pronounced strengthening, despite a lower volume fraction.[6]

IV. CONCLUSIONS

Partial isothermal sections of the Fe-Mo-Ti ternary system at 1173 K (900 °C) and 1023 K (750 °C) have been determined by examining a series of six bulk alloys. At both temperatures, extensive A2-B2 and A2-$D8_5$ two-phase fields were found to exist, with a narrow A2-C14 two-phase field between them. Across the A2-B2 two-phase field, the solubility for Fe in the A2 (Ti, Mo) phase was found to increase with both titanium content and temperature. The reduced solubility of Fe within the A2 phase with decreasing temperature may be exploited to create microstructures with fine B2 TiFe precipitates within an A2 matrix. To assess the extent to which such precipitation may occur, vertical sections between the A2 (Ti, Mo) and B2 TiFe phases were constructed, from which the maximum volume fraction of B2 TiFe precipitates that may be developed from an A2 matrix was calculated. This indicated that up to 40 pct, B2 TiFe precipitates can be produced in Fe-Mo-Ti ternary alloys with molybdenum contents of up to 20 at. pct.

ACKNOWLEDGMENTS

The authors would like to thank K. Roberts for his assistance and the Rolls-Royce/EPSRC Strategic Partnership for financial support under EP/H022309/1, EP/H500375/1, and EP/M005607/1.

REFERENCES

1. D.V. Louzguine, H. Kato, and A. Inoue: *J. Alloys Compd*, 2004, vol. 384, pp. L1–L3.
2. D.V. Louzguine-Luzgin, L.V. Louzguina-Luzgina, H. Kato, and A Inoue: *J. Alloys Compd*, 2007, vols. 434–435, pp. 32–35.
3. J. Das, K.B. Kim, F. Baier, W. Löser, A. Gebert, and J. Eckert: *J. Alloys Compd*, 2007, vols. 434–435, pp. 28–31.
4. J. Das, R. Theissmann, W. Löser, and J. Eckert: *J. Mater. Res.*, 2010, vol. 25, pp. 943–56.
5. G.H. Cao, Y.F. Peng, N. Liu, X. Li, Z.S. Lei, Z.M. Ren, D. Gerthsen, and A.M. Russell: *Mater. Sci. Eng. A*, 2014, vol. 609A, pp. 60–64.
6. A.J. Knowles, N.G. Jones, C.N. Jones, and H.J. Stone: *The 13th World Conference on Titanium proceedings*, 2015, pp. 1231–36. DOI:10.1002/9781119296126.ch209.
7. ZP Jin and C Qiu: *Metall. Trans. A.*, 1993, vol. 24A, pp. 2137–44.
8. A.J. Knowles, N.G. Jones, O.M.D.M. Messé, J.S. Barnard, C.N. Jones, and H.J. Stone: *Int. J. Refract. Met. Hard Mater.*, 2016, vol. 60, pp. 160–68.
9. V Raghavan: *J. Phase Equilib.*, 2003, vol. 24, pp. 182–83.
10. V Raghavan: *Phase Diagrams of Ternary Iron Alloys Part 6*, Indian Institute of Metals, Calcutta, 1992, pp. 994–96.
11. E.M. Sokolovskaya, E.F. Kazakova, B.I. Gryzunov, M. Duisebaev, and B.K. Konysova: *Vestn. Mosk. Univ. Ser. 2: Khim.*, 1988, vol. 43, pp. 404–05.
12. A KamegawaH, H Kudo, and M. Okada Takamura: *J. Jpn. Inst. Met. Mater.*, 2003, vol. 44, pp. 991–94.
13. A.K. Shurin, G.P. Dmitrieva, and T.S. Cherepova: *Powder Metall. Met. Ceram.*, 2003, vol. 42, pp. 513–16.
14. J. English: Binary and Ternary Phase Diagrams of Columbium, Molybdenum, Tantalum, and Tungsten, Defense Metals Information Center, 1961, pp. 150–52.
15. G.I. Nosova, N.B. D'yakonova, and I.V. Lyasotskii: *Met. Sci. Heat Treat.*, 2006, vol. 48, pp. 427–32.
16. S.K. Sikka, Y.K. Vohra, and R. Chidambaram: *Prog. Mater Sci.*, 1982, vol. 27, pp. 245–310.
17. LFS Dumitrescu, M Hillert, and N Sounders: *J. Phase Equilib.*, 1998, vol. 19, pp. 441–48.
18. P. Franke, and D. Neuschütz: Binary Systems. Part 4: Binary Systems from Mn-Mo to Y-Zr - Mo-Ti. Springer, Berlin, 2006.
19. J HouserováJ, J Vřešťál, and M Šob: *Calphad*, 2005, vol. 29, pp. 133–39.
20. J.L. Murray: *Bull. Alloy Phase Diagr.*, 1981, vol. 2, pp. 320–34.
21. R.J. Van Thyne, H.D. Kessler, and M. Hansen: *Trans. Am. Soc. Met.*, 1952, vol. 44, pp. 974–89.
22. V.B. Rajkumar and K.C.H. Kumar: *J. Alloys Compd.*, 2014, vol. 611, pp. 303–12.
23. C.P. Heijwegen and G.D. Rieck: *J. Less-Common Met.*, 1974, vol. 37, pp. 115–21.
24. H Bo, J Wang, L Duarte, C Leinenbach, L Liu, H Liu, and Z Jin: *Trans. Nonferrous Met. Soc. China.*, 2012, vol. 22, pp. 2204–11.